

Symmetry Enhanced Unconventional Spin Current Anisotropy in a Collinear Antiferromagnet

Pankhuri Gupta^{1†}, Kacho Imtiyaz Ali Khan^{1†,‡}, Akash Kumar^{2,3},
 Rekha Agarwal¹, Nidhi Kandwal¹, Ram Singh Yadav¹,
 Johan Åkerman^{2,3*} and Pranaba Kishor Muduli^{1*}

¹Department of Physics, Indian Institute of Technology Delhi, Hauz Khas,
 110016, New Delhi, India

²Department of Physics, University of Gothenburg, Fysikgränd 3,
 412 96, Gothenburg, Sweden

³Research Institute of Electrical Communication, Tohoku University, 2-1-1 Katahira,
 Aoba-ku, Sendai 980-8577 Japan

[†]These authors contributed equally to this work.

[‡]Present address: Paul-Drude-Institut für Festkörperelektronik,
 Leibniz-Institut im Forschungsverbund Berlin e.V., 10117 Berlin, Germany

*To whom correspondence should be addressed; E-mails:
 muduli@physics.iitd.ac.in, johan.akerman@physics.gu.se

Abstract

Spin-orbit torque (SOT) presents a promising avenue for energy-efficient spintronics devices, surpassing the limitations of spin transfer torque. While extensively studied in heavy metals, SOT in antiferromagnetic quantum materials remains largely unexplored. Here, we investigate SOT in epitaxial FeSn, a collinear antiferromagnet with a kagome lattice. FeSn exhibits intriguing topological quantum features, including two-dimensional flat bands and Dirac-like surface states, making it an ideal platform for investigating emergent SOT properties. Using spin-torque ferromagnetic resonance, we uncover a six-fold symmetric damping-like SOT in epitaxial-FeSn/Py heterostructures, reflecting the six-fold symmetry of the epitaxial [0001]-oriented FeSn films. Additionally, we observe a substantial unconventional field-like torque, originating from spin currents with out-of-plane spin polarization. This torque exhibits a unique angular dependence—a superposition of six-fold crystalline symmetry and uniaxial symmetry associated with the antiferromagnetic spin Hall effect. Notably, the unconventional field-like torque is enhanced when the RF current flows along the Néel vector in FeSn. Our findings reveal an unconventional spin current anisotropy tunable by crystalline and magnetic symmetry, offering a novel approach for controlling SOT in antiferromagnetic spintronics.

Spin-orbit torques (SOTs) have emerged as a powerful tool for a wide range of spintronic applications, including ultrafast magnetization switching [1, 2, 3], spintronic oscillators [4, 5, 6], and the emerging field of

spintronic-based neuromorphic computing [7, 8, 9, 10]. In commonly employed ferromagnet/heavy metal (FM/HM) heterostructures, SOTs are generated either through the spin Hall effect [11, 12] from the HM or the Rashba-Edelstein effect [13, 14] from the interface. In both cases, a charge current flowing in the x -direction produces a transverse spin current in the z -direction with spin polarization along the y -direction, a symmetry commonly referred to as “conventional SOT”, with *e.g.* the widely used material Pt and its isotropic SHE the most typical example [15, 16]. Here, isotropic SHE refers to the fact that the spin Hall conductivity is independent of the relative orientation of the current direction with respect to the crystallographic axis. Conventional SOT in ferromagnetic/heavy-metal heterostructures generate an in-plane anti-damping SOT, which cannot produce deterministic switching of perpendicularly magnetized systems used in high-density magnetic memory. [1, 2, 17, 18, 19].

Recent advancements in the field of quantum materials have led to the discovery of novel SOTs in two-dimensional (2D) materials and non-collinear antiferromagnets [20, 21]. These materials possess unique symmetry properties that facilitate the generation of unconventional SOT, characterized by spin polarization components along all three spatial axes, irrespective of the current direction. It has been demonstrated that symmetry breaking in 2D quantum materials such as WTe_2 [22, 23], and MoTe_2 [24] enables the emergence of such unconventional SOT. Furthermore, non-collinear kagome antiferromagnets like Mn_3GaN [25], Mn_3SnN [26], and Mn_3Sn [27], offer an alternative platform for realizing unconventional SOTs due to their low magnetic symmetry. For all these systems, SOT is intrinsically anisotropic due to its dependence on crystalline and/or magnetic symmetry. Recent studies have shown that similar to non-collinear kagome antiferromagnets, collinear kagome antiferromagnetic materials such as Mn_2Au , CuMnAs , and RuO_2 have the potential to generate out-of-plane spin polarization due to the broken space-reversal symmetries of the spin sublattice [28, 29].

Kagome antiferromagnetic materials constitute a distinctive class of quantum materials that have garnered significant attention due to their potential to host massless Dirac states [30]. These topological electronic states arise from the unique kagome lattice structure and the strong spin-orbit coupling [31, 32, 33]. FeSn is a collinear kagome antiferromagnet with a hexagonal structure (space group: $P6/mmm$) and a Néel temperature of 368 K [31, 34, 35]. The crystal structure of FeSn [as shown in Fig. 1a&b] consists of alternating kagome layers of Fe_3Sn and stanene layers of Sn_2 , which is slightly different from its kagome ferromagnet Fe_3Sn_2 , where two kagome layers are sandwiched between the stanene layers [36, 37]. However, within each kagome layer of FeSn , Fe atoms align ferromagnetically, while each kagome layer is antiferromagnetically coupled with each other via the stanene Sn_2 layer along the c -axis. Recently, Z. Lin *et al.* [31] have demonstrated massless Dirac fermions in bulk FeSn , due to the presence of a preserved combined PT symmetry, despite the individual breaking of P (space inversion) and T (time-reversal) symmetries. In addition, the geometrical configuration of Fe atoms present in kagome layers shows the co-existence of both bulk and surface Dirac fermions, as well as topological flat bands [31, 32]. Recent theoretical work by J. M. Dueñas [38] indicates the existence of both *intrinsic* DL torque and the FL torque arising from the bulk electronic structure of Dirac semimetals. Han *et al.* [39] experimentally observed surface states and proposed that these surface states can manifest peculiar SOTs, although any experimental confirmation has yet to be reported. These promising studies suggest that interfacing a kagome antiferromagnet FeSn with a conventional ferromagnet is expected to transfer strong and unconventional SOT across the interface. This remains an unexplored territory in terms of both experiments and theory. Therefore, exploring the spin-orbit torques (SOTs) in a heterostructure of Dirac semimetals, FeSn , and ferromagnets such as Py is highly interesting.

In this study, we optimize the deposition of high-quality epitaxial thin films of the antiferromagnet FeSn , utilizing a Pt seed layer on a c -plane Al_2O_3 substrate. Spin-torque ferromagnetic resonance (STFMR) mea-

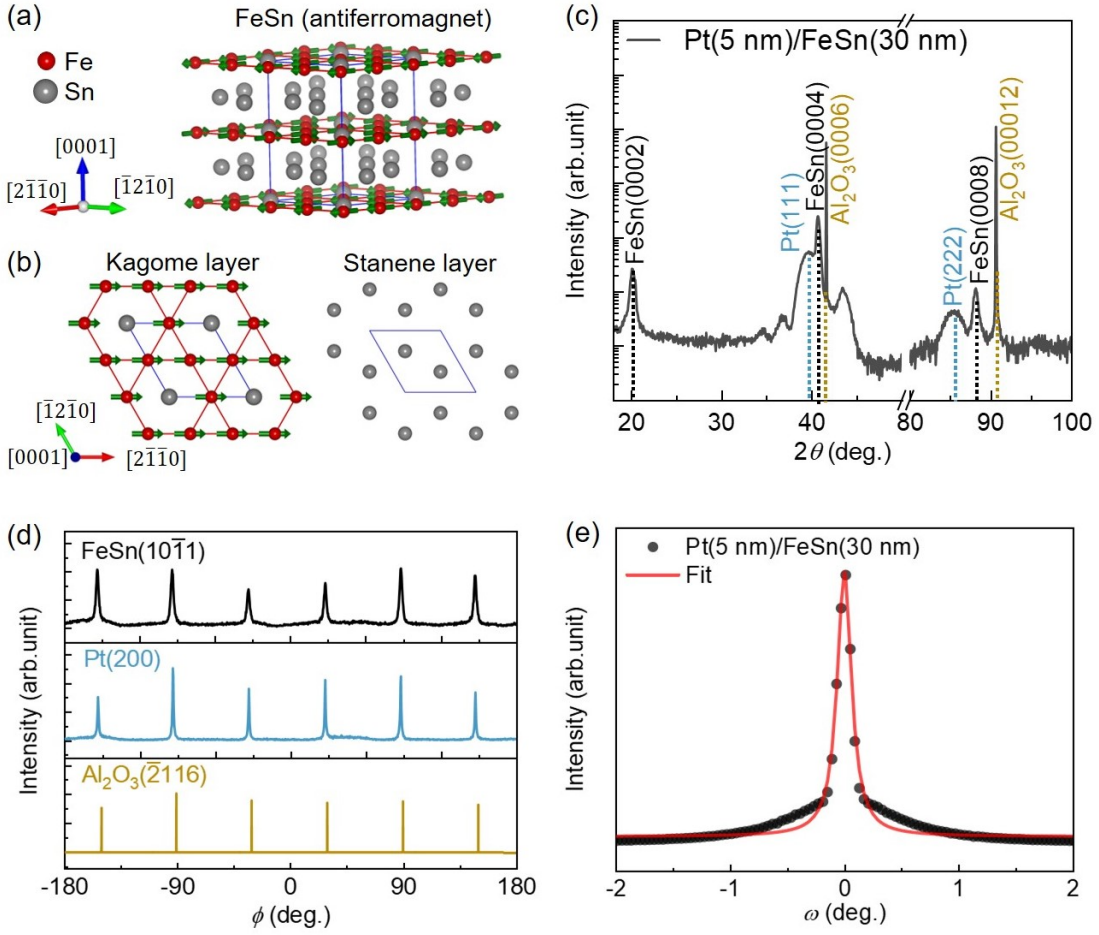


Figure 1: **Schematic of FeSn and XRD measurements** (a) Schematic of the unit cell (blue) of the kagome antiferromagnet FeSn. (b) Schematic of the kagome layer of Fe₃Sn and stanene layer of Sn₂. Fe atoms are depicted in red, and Sn atoms are shown in Gray. (c) Structural characterization using $\theta - 2\theta$ XRD scan measured for Pt(5 nm)/FeSn(30 nm). (d) ϕ -scan measurements for Pt(5 nm)/FeSn(30 nm) film on an Al₂O₃ substrate. The top, middle, and bottom panels show the ϕ -scans for FeSn(10 $\bar{1}$ 1), Pt(200), and Al₂O₃($\bar{2}$ 116) reflections, respectively. (e) The rocking curve (ω -scan) for the Pt(5 nm)/FeSn(30 nm). The black symbol and red line represent the measured data and fitted line to the ω -scan, respectively.

measurements on FeSn/Py heterostructure reveal the presence of a conventional damping-like (DL) torque due to the y -spin polarization (with efficiency: ξ_{DL}^y). Additionally, we observe a large unconventional field-like (FL) torque arising from the out-of-plane z -spin polarization (with efficiency: ξ_{FL}^z). Our results reveal that the observed six-fold symmetry of ξ_{DL}^y in FeSn/Py is directly correlated with the six-fold crystal symmetry of the [0001]-oriented FeSn films. Additionally, ξ_{FL}^z displays a unique angular dependence, characterized by a combination of the six-fold symmetry inherent to the FeSn crystal structure and the uniaxial symmetry associated with the antiferromagnetic spin Hall effect. Notably, the unconventional field-like torque is enhanced when the radio frequency (RF) current is aligned with the Néel vector.

1 Results and Discussion

1.1 Structural characterization

Figure 1c shows the XRD measurements performed in $\theta - 2\theta$ mode for a Pt(5 nm)/FeSn(30 nm) film stack. We see strong Bragg reflections at $2\theta = (20.1^\circ, 40.7^\circ, 88.2^\circ)$ corresponding to the FeSn(000 l) ($l = 2, 4, 8$) planes. The presence of peaks corresponding to only (000 l) planes indicates the epitaxial growth of FeSn layer, which was later confirmed by ϕ -scans. The additional peaks observed at $2\theta = 39.8^\circ$, and 85.4° correspond to Pt(111), and Pt(222) reflections, respectively. This confirms the epitaxial growth of the Pt layer on the c -plane Al₂O₃ substrate. In addition, we observed Laue oscillations at $2\theta = 34.5^\circ, 36.7^\circ$, and 43.4° , indicating a high interfacial quality of the seed layer as well as the FeSn layer [40].

To determine the epitaxial relation between the FeSn layer, the seed layer, and the substrate, we performed ϕ -scans on Pt(5 nm)/FeSn(30 nm) thin film stacks as shown in Fig 1d. For the ϕ -scan of the FeSn layer, we use the asymmetric reflection (10 $\bar{1}1$), which is observed at a tilt angle, $\chi = 45.04^\circ$ and $2\theta = 27.80^\circ$. For the Pt layer, we use the reflection (200), which is observed at $\chi = 54.7^\circ$ and $2\theta = 46.32^\circ$. At last, for Al₂O₃, we use the reflection ($\bar{2}116$), which is observed at $\chi = 41.86^\circ$ and $2\theta = 57.53^\circ$. The presence of six peaks in the ϕ -scan for Al₂O₃($\bar{2}116$) (bottom panel), Pt(200) (middle panel), and FeSn(10 $\bar{1}1$) (top panel) layers indicates a six-fold symmetry for both the Pt [41, 42, 43] and FeSn layers [44, 45]. For the Pt layer, the six-fold symmetry indicates the formation of twin domains (T₁, T₂) with 180° rotation around the Pt[111] pole with each other [41]. Therefore, the in-plane epitaxial relationship corresponding to Pt T₁- and T₂-domains are Al₂O₃[2 $\bar{1}\bar{1}0$] || Pt[1 $\bar{2}1$] || FeSn[2 $\bar{1}\bar{1}0$] and Al₂O₃[2 $\bar{1}\bar{1}0$] || Pt[$\bar{1}2\bar{1}$] || FeSn[2 $\bar{1}\bar{1}0$], respectively [41]. The out-of-plane crystallographic relation is found to be Al₂O₃[0001] || Pt[111] || FeSn[0001], which agrees with previous reports [44]. Furthermore, we performed ω -scans (rocking curves) on the FeSn (0004) reflection at $2\theta = 40.81^\circ$ [Fig 1e]. The value of the full width at half-maximum (FWHM) of the ω -scan is about 0.152° (≈ 547 arc-sec) for the FeSn (0004) reflection, indicating a high crystalline quality of the epitaxial FeSn layer grown on top of the Pt seed layer. The value of FWHM for our FeSn film is consistent with previous reports for a 30 nm-FeSn layer grown on top of Fe and Co seed layers [45]. Further, to confirm the antiferromagnetic nature of our FeSn film, we measured the exchange bias (H_{ex}) in a FeSn(30 nm)/Py(8 nm) bilayer, where the Py layer was deposited on top of the FeSn layer. The hysteresis loop of the ferromagnetic Py layer was initially recorded at room temperature ($T = 300$ K) and subsequently at a low temperature ($T = 2$ K) after cooling in the presence of a positive in-plane magnetic field of 60 kOe. At $T = 2$ K, a negative shift of approximately 52 Oe in the in-plane hysteresis loop was observed for the FeSn(30 nm)/Py(8 nm) bilayer, confirming the antiferromagnetic behavior of the FeSn film. H_{ex} almost doubles (~ 100 Oe) on reducing the Py thickness to 5 nm confirming the interfacial nature of the exchange bias.

1.2 STFMR measurements on FeSn/Py

To determine SOTs in the FeSn/Py bilayer, we performed STFMR measurements by passing an RF current (I_{RF}) through the devices, which induces alternating torques on the magnetization of the ferromagnet Py, exciting its resonance, as illustrated in Fig. 2a. We used a bias tee to apply an RF current with power +10 dBm from a signal generator, while simultaneously measuring the DC voltage. The STFMR signal was obtained by sweeping an in-plane magnetic field (H) through the resonance condition. More details of the measurement setup can be found elsewhere [46, 47]. Examples of STFMR spectra measured at different RF frequencies for

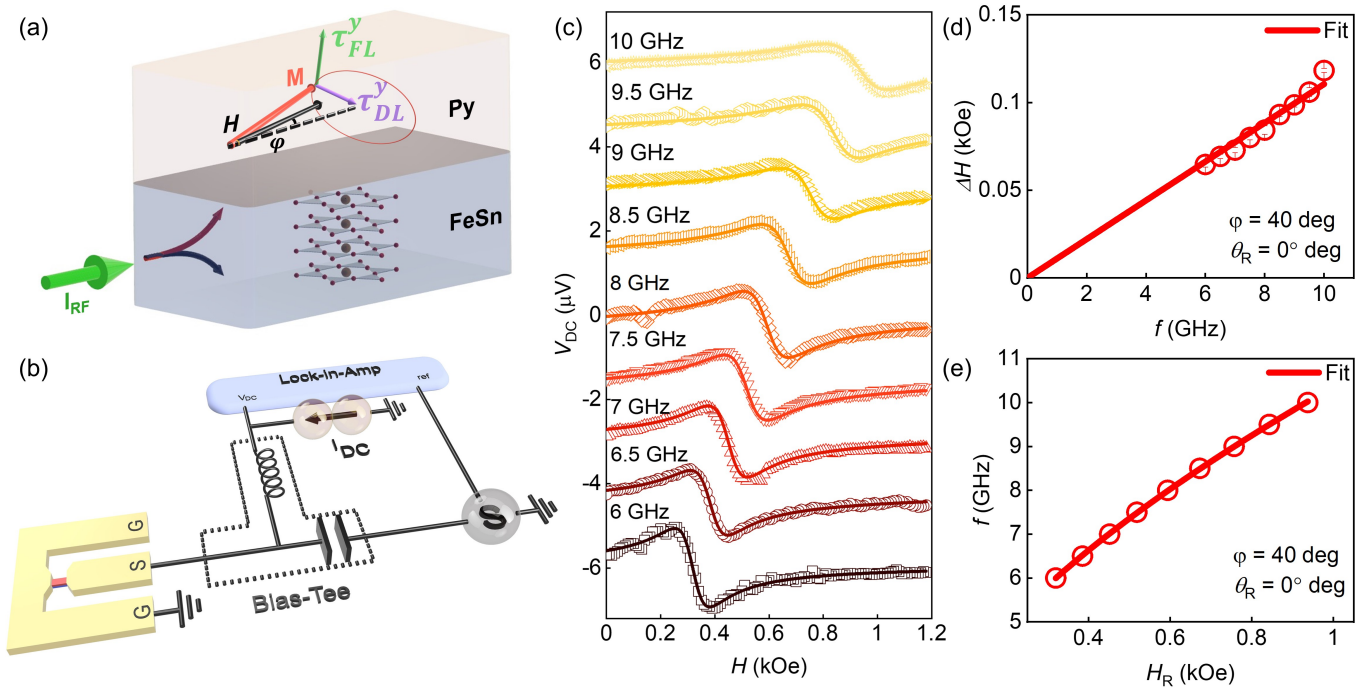


Figure 2: **STFMR measurements** (a) Structure of STFMR device consisting of a FeSn/Py bilayer. This device is subject to electric current flowing along the x -direction, resulting in the generation of both in-plane (τ_{\parallel}) and out-of-plane (τ_{\perp}) torque. (b) The schematic depicts the setup for STFMR measurements. (c) Frequency-dependent STFMR spectra of FeSn/Py microstrip measured at $\varphi = 40^\circ$ when the current direction is at 0° with in-plane reference direction $[1\bar{1}00]$ (The plots are shifted along the y -axis for clarity). (d) linewidth vs. frequency data and (e) frequency vs. resonance field data for FeSn/Py. Symbols are measured data, and solid lines are fits.

$\varphi = 40^\circ$ (the angle between H and I_{RF}) are shown in Fig. 2b. The angle, φ , was varied from 0° to 360° using a vector field magnet. Fits to the STFMR signal (V_{DC}) were performed using a combination of symmetric and antisymmetric Lorentzian functions: [48]

$$V_{\text{DC}} = V_{\text{S}} \frac{\Delta H^2}{\Delta H^2 + (H - H_{\text{R}})^2} + V_{\text{A}} \frac{\Delta H(H - H_{\text{R}})}{\Delta H^2 + (H - H_{\text{R}})^2}. \quad (1)$$

Here, V_{S} and V_{A} correspond to the magnitudes of the symmetric and anti-symmetric components of V_{DC} , proportional to the in-plane (τ_{\parallel}) and out-of-plane (τ_{\perp}) torques, respectively. In systems with conventional SHE and REE, the torques τ_{\parallel} and τ_{\perp} take the forms of $\hat{m} \times (\hat{m} \times \hat{y})$ and $\hat{m} \times \hat{y}$, respectively. Here, \hat{m} and \hat{y} represent the direction of the Py magnetization and the polarization of the spin current, respectively. Figure 2c shows the linewidth (ΔH) vs. RF frequency (f), fitted using $\Delta H = \frac{2\pi\alpha}{\gamma} f + \Delta H_0$ to obtain the Gilbert damping constant, $\alpha = 0.039 \pm 0.002$, and the inhomogeneous broadening, ΔH_0 [49, 50]. The strong enhancement in damping constant is due to a significant spin pumping from Py into kagome antiferromagnet FeSn [51]. The inhomogeneous broadening, ΔH_0 , was negligible, indicating a high film quality. Figure 2d illustrates the relationship between the frequency and the resonance field, from which the effective magnetization ($\mu_0 M_{\text{eff}}$) was extracted to (1.06 ± 0.01) T by fitting the data to the Kittel formula [23, 48]. This value indicates that there is no significant difference in magnetic properties of the Py layers grown on FeSn.

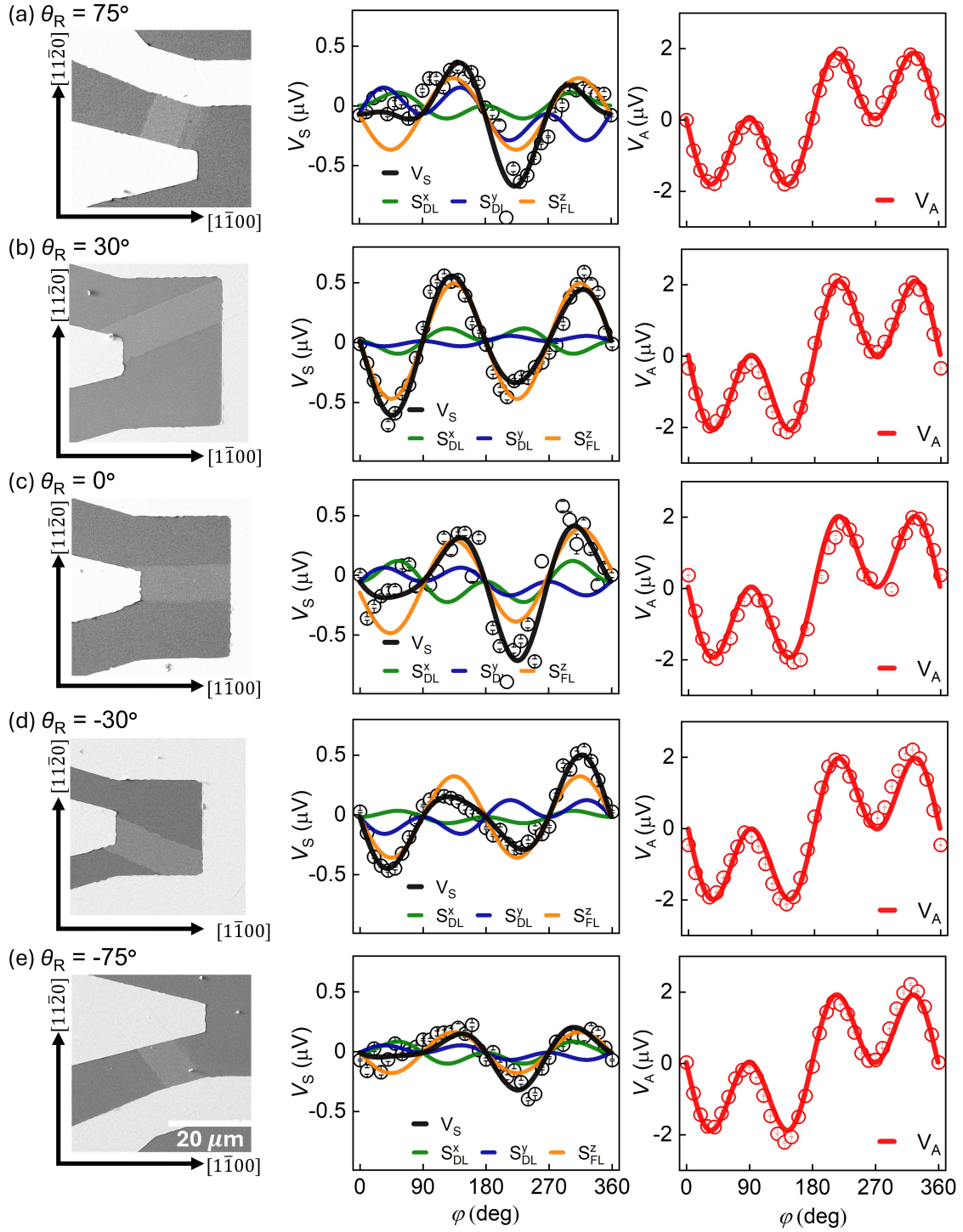


Figure 3: **Crystallographic dependence of STFMR** (a-e) SEM image of differently oriented devices (left panel), V_S (middle panel) and V_A (right panel) components as a function of angle φ . θ_R represent the angle between I_{RF} and in-plane reference direction $[1\bar{1}00]$.

We then analyze the results in more detail by performing complete angular dependence of the STFMR. In systems with conventional SHE and REE, the angular dependence of both the symmetric (V_S) and anti-symmetric voltage components (V_A) of the rectified voltage follow a $\sin(2\varphi)\sin(\varphi)$ behavior. Since FeSn is epitaxial, the STFMR measurements are carried out in FeSn/Py devices for I_{RF} along different angles (θ_R) with respect to

the Al_2O_3 crystal structure in-plane reference $[1\bar{1}00]$ direction: $\theta_R = 75^\circ, 30^\circ, 0^\circ, -30^\circ$ and -75° as shown in the left panel optical images of Fig. 3. The middle and right panels of Fig. 3 show the angular dependence for the symmetric (black) and antisymmetric (red) STFMR signals, respectively. The antisymmetric component clearly follows the conventional $\sin(2\varphi)\cos(\varphi)$ -dependence. In contrast, the symmetric component differs significantly from the conventional $\sin(2\varphi)\cos(\varphi)$ -behavior [23, 48]. Furthermore, the behavior changes dramatically with θ_R . To account for this deviation, extra terms proportional to $\sin(2\varphi)\sin(\varphi)$ and $\sin(2\varphi)$ are introduced, corresponding to spin polarizations in the x - and z -directions, respectively. The angular dependence of V_S and V_A for the reference sample showing the expected conventional $\sin(2\varphi)\cos(\varphi)$ -dependence. The angular dependence of V_S and V_A are fitted using [23, 25, 52]:

$$V_S \propto \sin(2\varphi) \left(S_{\text{DL}}^x \sin(\varphi) + S_{\text{DL}}^y \cos(\varphi) + S_{\text{FL}}^z \right) \quad (2)$$

$$V_A \propto A_{\text{FL}}^y \sin(2\varphi) \cos(\varphi) \quad (3)$$

Here, $S_{\text{DL}}^x \propto \hat{m} \times (\hat{m} \times \hat{x})$ and $S_{\text{DL}}^y \propto \hat{m} \times (\hat{m} \times \hat{y})$, both proportional to the DL torque component of the torque conductivity tensor, represent the unconventional component due to the \hat{x} spin polarization and the conventional component due to the \hat{y} spin polarization, respectively. Similarly, $A_{\text{FL}}^y \propto (\hat{m} \times \hat{y})$ and $S_{\text{FL}}^z \propto (\hat{m} \times \hat{z})$, represent the conventional component due to the \hat{y} spin polarization and the unconventional component due to the \hat{z} spin polarization, respectively. The superscript refers to the direction of the spin polarization for a charge current applied along \hat{x} .

By fitting the angular dependence of V_S and V_A with Eq. 2 and Eq. 3, the different torque components can be separated, with their efficiencies expressed as [52, 53]:

$$\xi_{\text{DL}}^x = \frac{S_{\text{DL}}^x}{A_{\text{FL}}^y} \frac{e\mu_0 M_{\text{StFM}} d_{\text{NM}}}{\hbar} \left[1 + \frac{4\pi M_{\text{eff}}}{H_{\text{R}}} \right]^{1/2} \quad (4)$$

$$\xi_{\text{DL}}^y = \frac{S_{\text{DL}}^y}{A_{\text{FL}}^y} \frac{e\mu_0 M_{\text{StFM}} d_{\text{NM}}}{\hbar} \left[1 + \frac{4\pi M_{\text{eff}}}{H_{\text{R}}} \right]^{1/2} \quad (5)$$

$$\xi_{\text{FL}}^z = \frac{S_{\text{FL}}^z}{A_{\text{FL}}^y} \frac{e\mu_0 M_{\text{StFM}} d_{\text{NM}}}{\hbar} \left[1 + \frac{4\pi M_{\text{eff}}}{H_{\text{R}}} \right]^{1/2} \quad (6)$$

Here, d_{NM} and t_{FM} are the non-magnetic and ferromagnetic layer thicknesses, respectively, and e the electric charge. The values of M_{eff} , H_{R} are calculated from the frequency-dependent STFMR measurements, as discussed above.

2 Crystallographic dependence of spin-torque efficiencies

Figure 4a shows the kagome structure with $\theta_R = -60^\circ$ and 30° , where the RF current is perpendicular and parallel to the Néel vector, respectively. The top and bottom panels in Fig. 4b&c show the measured DL and FL SOT efficiencies, respectively, as a function of θ_R in FeSn/Py and Ref. devices. The conventional DL SOT

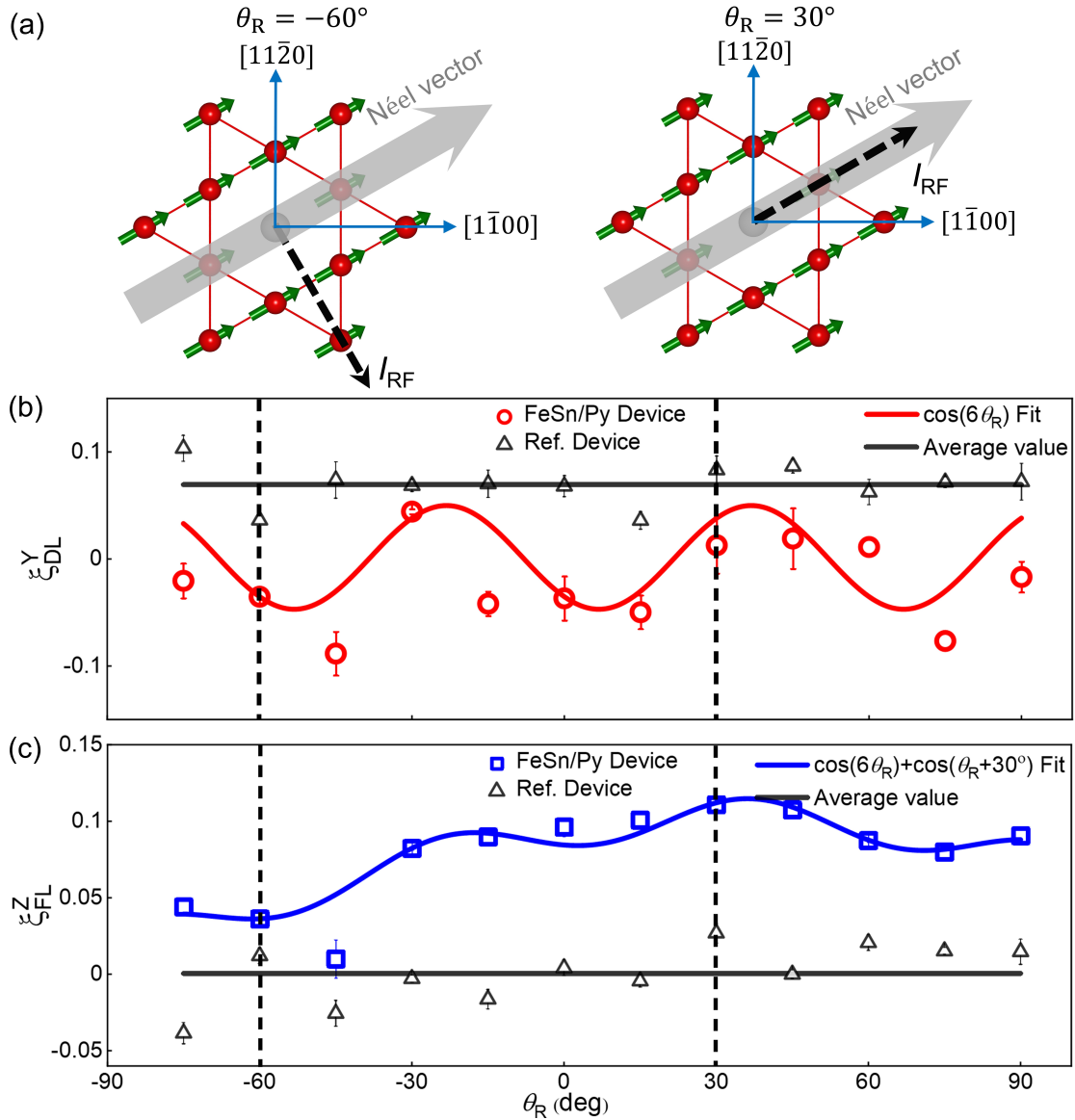


Figure 4: **Crystallographic dependence of spin-torque efficiencies** (a) Kagome Structure with Néel vector (gray) and I_{RF} (black dashed) in parallel and perpendicular orientations (b) DL SOT efficiency due to y - spin polarization and (c) FL SOT efficiency due to z - spin polarization for different θ_R values in FeSn/Py device and Ref. device.

efficiencies due to the y - spin polarization, denoted as ξ_{DL}^y , are shown in Fig. 4b for the Py/FeSn device and for the Ref. device. For the Ref. device, ξ_{DL}^y is independent of θ_R , which is expected for the isotropic SHE of Pt [54, 55]. In contrast, for the FeSn/Py heterostructure in Fig. 4b, ξ_{DL}^y exhibits a strong anisotropic behavior, and even sign inversions for different θ_R (different crystal axes), which are entirely absent in the Ref. device. The θ_R dependence of ξ_{DL}^y can be fitted using a $\cos(6\theta_R)$ function, illustrated by the red solid line in Fig. 4b. This fit indicates a six-fold symmetry in the SOT response, consistent with the underlying six-fold symmetry of the epitaxial [0001]-oriented FeSn films as observed in the ϕ -scan measurements [Fig. 1d]. Thus, ξ_{DL}^y can be linked to the bulk electronic properties of the FeSn kagome structure.

We also observe a large unconventional FL SOT due to the spin current with out-of-plane, or z -polarization, labeled as ξ_{FL}^z , as shown in Fig.4c. As expected, this unconventional torque, ξ_{FL}^z , is essentially absent in the

Ref. device. In contrast, for the FeSn/Py heterostructure, ξ_{FL}^z is not only large but also exhibits a strong anisotropic behavior, though there is no sign inversion of ξ_{FL}^z with θ_{R} unlike the case of ξ_{DL}^y . The θ_{R} dependence of ξ_{FL}^z can be modeled using a $\cos(6\theta_{\text{R}}) + \cos(\theta_{\text{R}} + 30^\circ)$ function, which is illustrated by the blue solid line in Fig. 4c. This fit indicates a combination of a six-fold symmetry and a uniaxial symmetry in the SOT response. The six-fold symmetry is consistent with the six-fold symmetry of the epitaxial [0001]-oriented FeSn films as observed in ξ_{DL}^y . However, the uniaxial term with a shift of 30° indicates the presence of an additional mechanism for the generation of out-of-plane spin current.

3 Discussion

In the following, we discuss the potential origin of the torques observed in FeSn/Py-based devices. FeSn is an antiferromagnetic kagome metal that exhibits exotic surface states. Han *et al.* [39] experimentally observed surface states and proposed that these surface states can manifest peculiar SOTs. Additionally, FeSn is a Dirac semimetal, and recent theoretical work by J. M. Dueñas [38] indicates the existence of both *intrinsic* DL torque and the FL torque arising from the bulk electronic structure of Dirac semimetals. The intrinsic torques originating from the band structure inherently possess anisotropic characteristics. Consequently, these torques are expected to exhibit a strong dependence on the crystallographic direction. The conventional DL torque, ξ_{DL}^y has strong anisotropic behavior with six-fold symmetry, consistent with X-ray measurements of the symmetry of epitaxial [0001]-oriented FeSn films. Therefore, the conventional DL torque, ξ_{DL}^y , can be attributed to an intrinsic origin arising from the topological features of the electronic band structure of FeSn. The presence of a six-fold component in the unconventional FL torque, ξ_{FL}^z , is also consistent with the above theoretical work [38], which predicts simultaneous enhancement of DL and FL torques.

The θ_{R} dependence of ξ_{FL}^z has an additional $\cos(\theta_{\text{R}} + 30^\circ)$ component. Our results suggest that ξ_{FL}^z also requires the presence of a FeSn layer adjacent to Py. Several recent studies have demonstrated the occurrence of an out-of-plane polarization resulting from the magnetic spin Hall effect in non-collinear antiferromagnets [56, 57, 58, 59]. Although FeSn is classified as a collinear antiferromagnet—which typically would not generate such torques—a recent investigation revealed the antiferromagnetic spin Hall effect in the collinear antiferromagnet, Mn_2Au [28]. They reported a FL torque arising from out-of-plane spin polarization when the current direction is parallel to the Néel vector. For FeSn, the Néel vector lies along the a -axis [60], as shown in Fig. 4a, which corresponds to $\theta_{\text{R}} = 30^\circ$. Therefore, we anticipate that for the antiferromagnetic spin Hall effect in FeSn, ξ_{FL}^z will be maximized at $\theta_{\text{R}} = 30^\circ$. Indeed, as shown in Fig. 4c, there is an observed increase in ξ_{FL}^z by over 50% $\theta_{\text{R}} = 30^\circ$ compared to $\theta_{\text{R}} = -60^\circ$, where the RF current is perpendicular to the Néel vector. This observation supports the conclusion that the uniaxial $\cos(\theta_{\text{R}})$ component can be attributed to the antiferromagnetic spin Hall effect. While the exact mechanism of the DL torque due to x -polarization ξ_{DL}^x , is not known, we believe it is also related to the interface between FeSn and Py since it does not exhibit a clear six-fold symmetry or uniaxial symmetry with θ_{R} .

4 Conclusion

In conclusion, we demonstrate successful epitaxial growth of high-quality FeSn thin films on c -plane Al_2O_3 substrate utilizing a Pt seed layer. A comprehensive investigation of spin-orbit torques (SOTs) in FeSn/Py

bilayers as a function of crystallographic orientation reveals a six-fold symmetric DL SOT and the coexistence of six-fold symmetric and uniaxial unconventional FL torques. The latter is attributed to the antiferromagnetic spin Hall effect, highlighting the unique potential of FeSn for SOT applications. The results highlight the unique properties of FeSn as a platform for exploring emergent SOT phenomena. By leveraging the topological features of FeSn and its interaction with adjacent ferromagnetic layers, all grown using industrially compatible co-sputtering, we anticipate that our results will inspire further exploration into antiferromagnetic spintronics relevant for direct SOT applications.

5 Experimental Details

5.1 Sample preparation

We prepared high-quality Pt(5 nm)/FeSn(30 nm)/Py(8 nm) multilayer film on *c*-plane Al₂O₃(0001) substrates using magnetron sputtering. The Pt layer's high quality was achieved with a growth rate of 0.27 Å s⁻¹ (RF power of 60 W) and a substrate temperature of 400 °C. The FeSn layer was grown using the co-sputtering technique. The sputtering rates of Fe and Sn targets were optimized by adjusting the power of each sputter gun to achieve the desired stoichiometry. Using 40 W of DC power for Fe and 85 W of RF power for Sn, we obtained a low net deposition rate of 0.4 Å s⁻¹ for the FeSn film. The FeSn layer was grown at a substrate temperature of 550 °C. The ferromagnetic Py layer (8 nm) was deposited at room temperature with a low growth rate of 0.25 Å s⁻¹ using 40 W of DC power. Additionally, we grew a reference sample (Ref): Pt(5 nm)/Py(10 nm) on *c*-plane Al₂O₃(0001) substrates (without FeSn layer) under the same growth conditions. Both samples were capped with an Al layer deposited at a growth rate of 0.20 Å s⁻¹ (RF power of 60 W). The base pressure of the sputtering chamber was better than 6.7×10⁻⁸ mbar, and the working pressure was maintained at 6.7×10⁻³ mbar. The substrate holder was rotated at 60 rpm during deposition to ensure better homogeneity of the films. After deposition, these samples have been patterned into microstrip devices of dimensions 40 μm long and 10 μm wide prepared by the lift-off technique using optical lithography.

5.2 Structural characterization

The actual stoichiometry of our Fe and Sn in FeSn thin films was found to be 50.2±0.5 at.% and 49.7±0.6 at.% by averaging the value at four different spots on the sample using the electronic probe microscopy analysis (EPMA) method. The $\theta - 2\theta$ (Gonio-XRD) and ϕ -scan XRD measurements have been used to investigate the epitaxial nature of the films. The high-resolution XRD measurements were performed using a PANalytical X'Pert diffractometer with Cu- K_α radiation ($\lambda = 1.5418$ Å).

5.3 STFMR measurements

We conducted STFMR measurements by applying an RF current using R&S signal generator (SMB 100A) with frequency, f at a constant RF power of +10 dBm to the device. The microstrip is connected via a Ground-signal-Ground probe. The RF signal was amplitude-modulated with a 98 Hz signal, and the resulting DC mixing voltage was detected with a lock-in amplifier (SR830). A bias tee is utilized to separate the DC and

RF port connected to the microstrip. An angle-dependent spin-torque ferromagnetic resonance (STFMR) was performed using vector field magnet to quantify the spin-orbit torque in the FeSn/Py system. The magnetic field was applied in the sample plane at an angle φ with respect to the current direction (x -direction) along the long axis of the microstrip. The angle, φ , was varied from ($0 - 360^\circ$) with the help of a vector field magnet (GMW 5201).

6 Declarations

The partial support from the Ministry of Human Resource Development under the IMPRINT program (Grants No. 7519 and No. 7058), the Department of Electronics and Information Technology (DeitY), the Science and Engineering Research Board (SERB File No. CRG/2018/001012 and No. CRG/2022/002821), Joint Advanced Technology Centre at IIT Delhi, Grand Challenge Project, IIT Delhi, and the Department of Science and Technology under the Nanomission program [grant no: *SR/NM/NT* – 1041/2016(*G*)], IEEE Magnetics Society Special Project [P.O. 502182] are gratefully acknowledged. We also acknowledge the Central Research Facility, IIT Delhi, for providing facilities for sample characterization.

Conflict of interest

The authors declare that there is no conflict of interest with respect to this paper.

References

- [1] Ioan Mihai Miron, Kevin Garello, Gilles Gaudin, Pierre Jean Zermatten, Marius V. Costache, Stéphane Auffret, Sébastien Bandiera, Bernard Rodmacq, Alain Schuhl, and Pietro Gambardella. Perpendicular switching of a single ferromagnetic layer induced by in-plane current injection. *Nature*, 476:189–193, Aug 2011.
- [2] L. Liu, C. F. Pai, Y. Li, H. W. Tseng, D. C. Ralph, and R. A. Buhrman. Spin-Torque Switching with the Giant Spin Hall Effect of Tantalum. *Science*, 336:555–558, May 2012.
- [3] Kevin Garello, Can Onur Avci, Ioan Mihai Miron, Manuel Baumgartner, Abhijit Ghosh, Stéphane Auffret, Olivier Boulle, Gilles Gaudin, and Pietro Gambardella. Ultrafast magnetization switching by spin-orbit torques. *Appl. Phys. Lett.*, 105:212402, 2014.
- [4] Vladislav E. Demidov, Sergei Urazhdin, Henning Ulrichs, Vasyl Tiberkevich, Andrei Slavin, Dietmar Baither, Guido Schmitz, and Sergej O. Demokritov. Magnetic nano-oscillator driven by pure spin-current. *Nat. Mater.*, 11:1028–1031, Oct 2012.
- [5] A. A. Awad, P. Dürrenfeld, A. Houshang, M. Dvornik, E. Iacocca, R. K. Dumas, and J. Åkerman. Long-range mutual synchronization of spin Hall nano-oscillators. *Nat. Phys.*, 13:292–299, nov 2017.

- [6] Akash Kumar, Avinash K. Chaurasiya, Nilamani González, Victor H. and Behera, Ademir Aléman, Roman Khymyn, Ahmad A. Awad, and Johan Åkerman. Spin-wave-mediated mutual synchronization and phase tuning in spin Hall nano-oscillators. *Nat. Phys.*, 21(242), January 2025.
- [7] Julie Grollier, Damien Querlioz, KY Camsari, Karin Everschor-Sitte, Shunsuke Fukami, and Mark D Stiles. Neuromorphic spintronics. *Nat. Electron.*, 3:360–370, 2020.
- [8] Afshin Houshang, Mohammad Zahedinejad, Shreyas Muralidhar, Roman Khymyn, Mona Rajabali, Himanshu Fulara, Ahmad A Awad, Johan Åkerman, Jakub Checiński, and Mykola Dvornik. Phase-Binarized Spin Hall Nano-Oscillator Arrays: Towards Spin Hall Ising Machines. *Phys. Rev. Appl.*, 17:014003, 2022.
- [9] Neha Garg, Sri Vasudha Hemadri Bhotla, Pranaba Kishor Muduli, and Debanjan Bhowmik. Kuramoto-model-based data classification using the synchronization dynamics of uniform-mode spin Hall nano-oscillators. *Neuromorph. Comput. Eng.*, 1:024005, 2021.
- [10] Ram S Yadav, Pankhuri Gupta, Amod Holla, Kacho Imtiyaz Ali Khan, Pranaba K Muduli, and Debanjan Bhowmik. Demonstration of Synaptic Behavior in a Heavy-Metal-Ferromagnetic-Metal-Oxide-Heterostructure-Based Spintronic Device for On-Chip Learning in Crossbar-Array-Based Neural Networks. *ACS Appl. Electron. Mater.*, 5:484–497, 2023.
- [11] M. I. Dyakonov and V. I. Perel. Current-induced spin orientation of electrons in semiconductors. *Phys. Lett. A*, 35:459–460, Jul 1971.
- [12] J. E. Hirsch. Spin Hall Effect. *Phys. Rev. Lett.*, 83:1834–1837, Aug 1999.
- [13] Yu A Bychkov and É I Rashba. Properties of a 2D electron gas with lifted spectral degeneracy. *JETP lett*, 39:78, 1984.
- [14] Victor M Edelstein. Spin polarization of conduction electrons induced by electric current in two-dimensional asymmetric electron systems. *Solid State Commun.*, 73:233–235, 1990.
- [15] Frank Freimuth, Stefan Blügel, and Yuriy Mokrousov. Anisotropic spin Hall effect from first principles. *Phys. Rev. Lett.*, 105:246602, 2010.
- [16] EM Chudnovsky. Intrinsic spin Hall effect in noncubic crystals. *Phys. Rev. B*, 80:153105, 2009.
- [17] G. Yu, P. Upadhyaya, Y. Fan, J. G. Alzate, W. Jiang, K. L. Wong, S. Takei, S. A. Bender, L. T. Chang, Y. Jiang, M. Lang, J. Tang, Y. Wang, Y. Tserkovnyak, P. K. Amiri, and K. L. Wang. Switching of perpendicular magnetization by spin-orbit torques in the absence of external magnetic fields. *Nat. Nano.*, 9:548–554, 2014.
- [18] Luqiao Liu, OJ Lee, TJ Gudmundsen, DC Ralph, and RA Buhrman. Current-induced switching of perpendicularly magnetized magnetic layers using spin torque from the spin Hall effect. *Phys. Rev. Lett.*, 109:096602, 2012.
- [19] Shunsuke Fukami, T Anekawa, C Zhang, and H Ohno. A spin-orbit torque switching scheme with collinear magnetic easy axis and current configuration. *Nat. Nano.*, 11:621–625, 2016.
- [20] Mingming Tian, Yonghui Zhu, Milad Jalali, Wei Jiang, Jian Liang, Zhaocong Huang, Qian Chen, Zhongming Zeng, and Ya Zhai. Two-dimensional van der Waals materials for spin-orbit torque applications. *Front. nanotechnol.*, 3:732916, 2021.

- [21] Cheng Song, Ruiqi Zhang, Liyang Liao, Yongjian Zhou, Xiaofeng Zhou, Ruyi Chen, Yunfeng You, Xianzhe Chen, and Feng Pan. Spin-orbit torques: Materials, mechanisms, performances, and potential applications. *Prog. Mater. Sci.*, 118:100761, 2021.
- [22] David MacNeill, Gregory M Stiehl, Marcos HD Guimaraes, Neal D Reynolds, Robert A Buhrman, and Daniel C Ralph. Thickness dependence of spin-orbit torques generated by WTe₂. *Phys. Rev. B*, 96:054450, 2017.
- [23] D. MacNeill, G. M. Stiehl, M. H. D. Guimaraes, R. A. Buhrman, J. Park, and D. C. Ralph. Control of spin-orbit torques through crystal symmetry in WTe₂/ferromagnet bilayers. *Nat. Phys.*, 13:300–305, Mar 2017.
- [24] Gregory M Stiehl, Ruofan Li, Vishakha Gupta, Ismail El Baggari, Shengwei Jiang, Hongchao Xie, Lena F Kourkoutis, Kin Fai Mak, Jie Shan, Robert A Buhrman, and Daniel C. Ralph. Layer-dependent spin-orbit torques generated by the centrosymmetric transition metal dichalcogenide β -MoTe₂. *Phys. Rev. B*, 100:184402, 2019.
- [25] Tianxiang Nan, Camilo X. Quintela, Julian Irwin, Gautam Gurung, Ding-Fu Shao, Jonathan Gibbons, Neil Campbell, Kyung Mee Song, Si-Young Choi, Lu Guo, R. D. Johnson, Pascal Manuel, Rajesh Vilas Chopdekar, Ingrid Hallsteinsen, Thomas Tybell, Philip J. Ryan, Jong-Woo Kim, Y. Choi, Paolo G. Radaelli, Daniel C. Ralph, E. Y. Tsymba, Mark S Rzchowski, and C. B. Eom. Controlling spin current polarization through non-collinear antiferromagnetism. *Nat. Commun.*, 11:4671, 2020.
- [26] Yunfeng You, Hua Bai, Xiaoyu Feng, Xiaolong Fan, Lei Han, Xiaofeng Zhou, Yongjian Zhou, Ruiqi Zhang, Tongjin Chen, Feng Pan, and Cheng Song. Cluster magnetic octupole induced out-of-plane spin polarization in antiperovskite antiferromagnet. *Nat. Commun.*, 12:6524, 2021.
- [27] Kouta Kondou, Hua Chen, Takahiro Tomita, Muhammad Ikhlas, Tomoya Higo, Allan H MacDonald, Satoru Nakatsuji, and YoshiChika Otani. Giant field-like torque by the out-of-plane magnetic spin Hall effect in a topological antiferromagnet. *Nat. Commun.*, 12:6491, 2021.
- [28] Xianzhe Chen, Shuyuan Shi, Guoyi Shi, Xiaolong Fan, Cheng Song, Xiaofeng Zhou, Hua Bai, Liyang Liao, Yongjian Zhou, Hanwen Zhang, Ang Li, Yanhui Chen, Xiaodong Han, Shan Jiang, Zengwei Zhu, Huaqiang Wu, Xiangrong Wang, Desheng Xue, Hyunsoo Yang, and Feng Pan. Observation of the antiferromagnetic spin Hall effect. *Nat. Mater.*, 20:800–804, 2021.
- [29] Rafael González-Hernández, Libor Šmejkal, Karel Výborný, Yuta Yahagi, Jairo Sinova, Tomáš Jungwirth, and Jakub Železný. Efficient Electrical Spin Splitter Based on Nonrelativistic Collinear Antiferromagnetism. *Phys. Rev. Lett.*, 126, Mar 2021.
- [30] Niru Chowdhury, Kacho Imtiyaz Ali Khan, Himanshu Bangar, Pankhuri Gupta, Ram Singh Yadav, Rekha Agarwal, Akash Kumar, and Pranaba Kishor Muduli. Kagome magnets: The emerging materials for spintronic memories. *Proc. Natl. Acad. Sci., India, Sect. A Phys. Sci.*, 93:477–495, 2023.
- [31] Zhiyong Lin, Chong Wang, Pengdong Wang, Seho Yi, Lin Li, Qiang Zhang, Yifan Wang, Zhongyi Wang, Haoran Huang, Yan Sun, Yaobo Huang, Dawei Shen, Donglai Feng, Zhe Sun, Jun-Hyung Cho, Changgan Zeng, and Zhenyu Zhang. Dirac fermions in antiferromagnetic FeSn kagome lattices with combined space inversion and time-reversal symmetry. *Phys. Rev. B*, 102:155103, 2019.

- [32] Zhiyong Lin, Jin Ho Choi, Qiang Zhang, Wei Qin, Seho Yi, Pengdong Wang, Lin Li, Yifan Wang, Hui Zhang, Zhe Sun, Laiming Wei, Shengbai Zhang, Tengfei Guo, Qingyou Lu, Jun Hyung Cho, Changgan Zeng, and Zhenyu Zhang. Flatbands and Emergent Ferromagnetic Ordering in Fe_3Sn_2 Kagome Lattices. *Phys. Rev. Lett.*, 121:096401, Aug 2018.
- [33] Himanshu Bangar, Kacho Imtiyaz Ali Khan, Akash Kumar, Niru Chowdhury, Prasanta Kumar Muduli, and Pranaba Kishor Muduli. Large spin Hall conductivity in epitaxial thin films of kagome antiferromagnet Mn_3Sn at room temperature. *Adv. Quantum Technol.*, 6:2200115, 2023.
- [34] L Haggstrom, T Ericsson, R Wappling, and K Chandra. Studies of the magnetic structure of FeSn using the Mossbauer effect. *Phys. Scr.*, 11:47, 1975.
- [35] Brian C Sales, Jiaqiang Yan, William R Meier, Andrew D Christianson, Satoshi Okamoto, and Michael A McGuire. Electronic, magnetic, and thermodynamic properties of the kagome layer compound FeSn. *Phys. Rev. Mater.*, 3:114203, 2019.
- [36] Kacho Imtiyaz Ali Khan, Ram Singh Yadav, Himanshu Bangar, Akash Kumar, Niru Chowdhury, Prasanta Kumar Muduli, and Pranaba Kishor Muduli. Intrinsic anomalous Hall effect in thin films of topological kagome ferromagnet Fe_3Sn_2 . *Nanoscale*, 14:8484–8492, 2022.
- [37] Kacho Imtiyaz Ali Khan, Akash Kumar, Pankhuri Gupta, Ram Singh Yadav, Johan akerman, and Pranaba Kishor Muduli. Magnetodynamic properties of ultrathin films of Fe_3Sn_2 -a topological kagome ferromagnet. *Sci. Rep.*, 14:3487, 2024.
- [38] Joaqun Medina Duenas, Jos H Garca, and Stephan Roche. Emerging Spin-Orbit Torques in Low-Dimensional Dirac Materials. *Phys. Rev. Lett.*, 132:266301, 2024.
- [39] Minyong Han, Hisashi Inoue, Shiang Fang, Caolan John, Linda Ye, Mun K Chan, David Graf, Takehito Suzuki, Madhav Prasad Ghimire, Won Joon Cho, Efthimios Kaxiras, and Joseph G. Checkelsky. Evidence of two-dimensional flat band at the surface of antiferromagnetic kagome metal FeSn. *Nat. Commun.*, 12:5345, 2021.
- [40] Shuyu Cheng, Binbin Wang, Igor Lyalin, Nria Bagues, Alexander J Bishop, David W McComb, and Roland K Kawakami. Atomic layer epitaxy of kagome magnet Fe_3Sn_2 and Sn-modulated heterostructures. *APL Mater.*, 10:061112, 2022.
- [41] Shun’ichiro Kurosawa, Tomoya Higo, Shota Saito, Ryota Uesugi, and Satoru Nakatsuji. Large spontaneous magneto-thermoelectric effect in epitaxial thin films of the topological kagome ferromagnet Fe_3Sn . *Phys. Rev. Mater.*, 8:054206, 2024.
- [42] Ken Verguts, Yves Defossez, Alessandra Leonhardt, Joke De Messemaeker, Koen Schouteden, Chris Van Haesendonck, Cedric Huyghebaert, Stefan De Gendt, and Steven Brems. Growth of millimeter-sized graphene single crystals on Al_2O_3 (0001)/Pt (111) template wafers using chemical vapor deposition. *ECS J Solid State Sci Technol*, 7:M195, 2018.
- [43] Hans F Wardenga and Andreas Klein. Surface potentials of (111),(110) and (100) oriented CeO_{2-x} thin films. *Appl. Surf. Sci.*, 377:1–8, 2016.
- [44] Durga Khadka, TR Thapaliya, Jiajia Wen, Ryan F Need, and SX Huang. High quality epitaxial thin films and exchange bias of antiferromagnetic Dirac semimetal FeSn. *Appl. Phys. Lett.*, 117:032403, 2020.

- [45] Prajwal M Laxmeesha, Tessa D Tucker, Rajeev Kumar Rai, Shuchen Li, Myoung-Woo Yoo, Eric A Stach, Axel Hoffmann, and Steven J May. Epitaxial growth and magnetic properties of kagome metal FeSn/elemental ferromagnet heterostructures. *J. Appl. Phys.*, 135:085302, 2024.
- [46] Akash Kumar, Raghav Sharma, Kacho Imtiyaz Ali Khan, Chandrasekhar Murapaka, Gerard Joseph Lim, Wen Siang Lew, Sujeet Chaudhary, and Pranaba Kishor Muduli. Large Damping-like Spin–Orbit Torque and Improved Device Performance Utilizing Mixed-Phase Ta. *ACS Appl. Electron. Mater.*, 3:3139–3146, 2021.
- [47] Akash Kumar, Pankhuri Gupta, Niru Chowdhury, Kacho Imtiyaz Ali Khan, Utkarsh Shashank, Surbhi Gupta, Yasuhiro Fukuma, Sujeet Chaudhary, and Pranaba Kishor Muduli. Interfacial Origin of Unconventional Spin-Orbit Torque in Py/ γ - γ -IrMn₃. *Adv. Quantum Technol.*, 6:2300092, 2023.
- [48] Luqiao Liu, Takahiro Moriyama, DC Ralph, and RA Buhrman. Spin-torque ferromagnetic resonance induced by the spin Hall effect. *Phys. Rev. Lett.*, 106:036601, 2011.
- [49] Richa Mudgal, Alka Jakhar, Pankhuri Gupta, Ram Singh Yadav, Bubunu Biswal, Pratik Sahu, Himanshu Bangar, Akash Kumar, Niru Chowdhury, Biswarup Satpati, et al. Magnetic-Proximity-Induced Efficient Charge-to-Spin Conversion in Large-Area PtSe₂/Ni₈₀Fe₂₀ Heterostructures. *Nano Lett.*, 23:11925–11931, 2023.
- [50] Pankhuri Gupta, Niru Chowdhury, Mingran Xu, Prasanta Kumar Muduli, Akash Kumar, Kouta Kondou, Yoshichika Otani, and Pranaba Kishor Muduli. Generation of out-of-plane polarized spin current in (permalloy, Cu)/EuS interfaces. *Phys. Rev. B*, 109:L060405, 2024.
- [51] Kacho Imtiyaz Ali Khan and Pranaba Kishor Muduli. Giant spin pumping enhancement at the interface of ferromagnet (Py) and Kagome antiferromagnet (FeSn). *Under Prepration*.
- [52] Arnab Bose, Nathaniel J Schreiber, Rakshit Jain, Ding-Fu Shao, Hari P Nair, Jiaxin Sun, Xiyue S Zhang, David A Muller, Evgeny Y Tsymbal, Darrell G Schlom, and D C Ralph. Tilted spin current generated by the collinear antiferromagnet ruthenium dioxide. *Nat. Electron.*, 5:267–274, 2022.
- [53] Jing Zhou, Xinyu Shu, Yaohua Liu, Xiao Wang, Weinan Lin, Shaohai Chen, Liang Liu, Qidong Xie, Tao Hong, Ping Yang, Binghai Yan, Xiufeng Han, and Jingsheng Chen. Magnetic asymmetry induced anomalous spin-orbit torque in irmn. *Phys. Rev. B*, 101:184403, 2020.
- [54] Adrián Gudín, Alberto Anadón, Iciar Arnay, Rubén Guerrero, Julio Camarero, Sebastien Petit-Watelot, Paolo Perna, and Juan-Carlos Rojas-Sánchez. Isotropic spin and inverse spin Hall effect in epitaxial (111)-oriented Pt/Co bilayers. *Phys. Rev. Mater.*, 7:124412, 2023.
- [55] C Guillemard, S Petit-Watelot, S Andrieu, and J-C Rojas-Sánchez. Charge-spin current conversion in high quality epitaxial Fe/Pt systems: Isotropic spin Hall angle along different in-plane crystalline directions. *Appl. Phys. Lett.*, 113:262404, 2018.
- [56] Yang Zhang, Yan Sun, Hao Yang, Jakub Železný, Stuart PP Parkin, Claudia Felser, and Binghai Yan. Strong anisotropic anomalous Hall effect and spin Hall effect in the chiral antiferromagnetic compounds Mn₃X (X= Ge, Sn, Ga, Ir, Rh, and Pt). *Phys. Rev. B*, 95:075128, 2017.
- [57] Jakub Železný, Yang Zhang, Claudia Felser, and Binghai Yan. Spin-polarized current in noncollinear antiferromagnets. *Phys. Rev. Lett.*, 119:187204, 2017.

- [58] Motoi Kimata, Hua Chen, Kouta Kondou, Satoshi Sugimoto, Prasanta K. Muduli, Muhammad Ikhlas, Yasutomo Omori, Takahiro Tomita, Allan. H. MacDonald, Satoru Nakatsuji, and Yoshichika Otani. Magnetic and magnetic inverse spin Hall effects in a non-collinear antiferromagnet. *Nature*, 565:627–630, 2019.
- [59] Alexander Mook, Robin R Neumann, Annika Johansson, Jürgen Henk, and Ingrid Mertig. Origin of the magnetic spin Hall effect: Spin current vorticity in the Fermi sea. *Phys. Rev. Res.*, 2:023065, 2020.
- [60] Soumya Sankar, Ruizi Liu, Cheng-Ping Zhang, Qi-Fang Li, Caiyun Chen, Xue-Jian Gao, Jiangchang Zheng, Yi-Hsin Lin, Kun Qian, Ruo-Peng Yu, et al. Experimental Evidence for a Berry Curvature Quadrupole in an Antiferromagnet. *Phys. Rev. X*, 14:021046, 2024.